3-Dimensional Motion Recognition by 4-Dimensional Higher-order Local Auto-correlation

Hiroki Mori, Takaomi Kanda, Dai Hirose and Minoru Asada
Department of Adaptive Machine Systems, Graduate School of Engineering, Osaka University, Suita city, Osaka, Japan
{*hiroki, takaomi.kanda, dai.hirose, asada*}*@ams.eng.osaka-u.ac.jp*

Keywords: 4-Dimensional Pattern Recognition, Higher-order Local Auto-correlation, Point Cloud Time Series, Voxel Time Series, Tesseractic Pattern, IXMAS Dataset.

Abstract: In this paper, we propose a 4-Dimensional Higher-order Local Auto-Correlation (4D HLAC). The method aims to extract the features of a 3D time series, which is regarded as a 4D static pattern. This is an orthodox extension of the original HLAC, which represents correlations among local values in 2D images and can effectively summarize motion in 3D space. To recognize motion in the real world, a recognition system should exploit motion information from the real-world structure. The 4D HLAC feature vector is expected to capture representations for general 3D motion recognition, because the original HLAC performed very well in image recognition tasks. Based on experimental results showing high recognition performance and low computational cost, we conclude that our method has a strong advantage for 3D time series recognition, even in practical situations.

1 INTRODUCTION

Motion recognition has many important applications in fields such as video surveillance, robotics, human–computer interaction, and individual behavior analyses for marketing. Recognition systems should effectively exploit features from the real world that exist in space and time (4D space).

Most conventional methods for recognizing motion use the color or intensity time series from 2D images. However, such images suffer from a light condition and motion in the depth direction. Motion in 3D space, rather than motion in depth, must be considered to solve this difficulty with 2D images. However, there has been little research on the direct application of 3D time series to the wide variety of motion recognition applications.

In this paper, we propose a 4-Dimensional Higher-order Local Auto-Correlation (4D HLAC) that can represent pattern features in point-cloud time series data and tesseract array data (voxel-time series data). The concept of HLAC (Otsu and Kurita, 1988) can be applied to any data array to extract the features of the pattern. However, the original article on HLAC only considered 2D image data in which features are characterized by model-free, shift invariance, and additivity. HLAC can also be applied to 3D array data (Cubic HLAC, or CHLAC (Kobayashi and Otsu, 2004)) to handle 3D objects and 2D movies (2D images + time series). However, only 4D HLAC allows voxel time series to be directly recognized as a static object consisting of tesseracts in 4D space. We have conducted two experiments that apply 4D HLAC to human motion to examine the performance and computational cost of the method.

The remainder of this article proceeds as follows. Some related work in the field of 3D motion recognition is discussed in Section 2, and our proposed 4D HLAC feature is introduced in Section 3. Section 4 describes the experimental setup, and Section 5 compares our results with those from previous research based on the IXMAS dataset. Finally, we present our conclusions in Section 6.

2 RELATED WORK

In this section, we summarize related work on 3D motion recognition. 3D motion recognition is mainly performed in a multi-camera environment, whereby the motion of an object is captured by multiple cameras from different perspectives. Previous image features can be separated into two categories based on how many spatial dimensions they use: the raw 2D images from multiple cameras, or a reconstructed 3D representation.

One approach is to use 2D image processing techniques and features from multi-view cameras, such as spatiotemporal interest points (Wu et al., 2011) from 2D movies, and silhouette-based features (Cherla et al., 2008; Chaaraoui et al., 2014). Weinland et al. (2010) proposed a 3D modeling method that produces 2D image information for recognition. Following feature extraction, their method does not use 3D reconstruction in the recognition phase (Weinland et al., 2010).

Concepts based on 3D analysis tend to extract features from 3D data such as point clouds and voxel images. Previous studies of 3D motion features have proposed various techniques, such as a layered cylindrical Fourier transform around the subject's vertical axis (Weinland et al., 2006; Turaga et al., 2008), circular patterns intersecting the subject's body on horizontal planes, 4D spatiotemporal interest points (4D-STIP), and optical flows based on HoG to represent 3D motion (Holte et al., 2012).

Our approach in this paper is based on the idea of HLAC (Otsu and Kurita, 1988). After HLAC was applied to pattern recognition in static 2D images, 3D extensions of HLAC were proposed for the recognition of 2D movies as spatiotemporal patterns (Kobayashi and Otsu, 2004) and the recognition and retrieval of 3D objects (color cubic HLAC, or CCHLAC (Kanezaki et al., 2010)). To use CHLAC for 2D movies, a layered 2D image that changes with time is considered to represent a 3D object in the spatiotemporal domain. This extension from HLAC to CHLAC inspired the idea of 4D HLAC. A comparison of the different HLAC variations is shown in Figure 2. In the next section, we give a definition of HLAC, describe its extension to four dimensions, and identify certain characteristics and theoretical expectations for 4D HLAC.

3 4D HLAC

3.1 Basic Idea of HLAC

The Nth-order auto-correlation function is defined as

$$h(a_1,\ldots,a_N) = \int f(r)\cdot f(r+a_1)\cdot\ldots\cdot f(r+a_N)dr, \tag{1}$$

where r is a reference vector in an image and $a_i(i = 1,\ldots,N)$ are displacement vectors based on r. A feature x is defined by the order of N and the displacements a_i. Therefore, a feature vector consists of all possible variations of h, with a constraint on the maximum size of N and the distance between a and r. Finally, any equivalent variations are eliminated.

In practical terms, Equation (1) should be discretized into

$$\begin{aligned} h = \underbrace{\sum_i \ldots \sum_l}_{D} & I(i,\ldots,l)\cdot I(i+a_1[1],\ldots,l+a_1[D])\cdot\ldots \\ & \cdot I(i+a_N[1],\ldots,l+a_N[D]), \end{aligned} \tag{2}$$

where $I(i,\ldots,j)$ is a D-dimensional image, meaning the summation is applied D times. The set of vectors $a_1 \ldots a_N$ represents one of the higher-order correlation patterns. The term $a_k[\cdot]$ represents an element of the vector a_k. In light of previous HLAC research (Otsu and Kurita, 1988; Kobayashi and Otsu, 2004), we assume that the order N is less than or equal to 2, and the range of the displacement is defined by a local $3\times\cdots\times 3$ region. HLAC masks for 2D images are shown in Figure 1. One of the patterns for $N = 2$ is represented by $a_1 = (1,0), a_2 = (1,1)$ in the top-left image of Figure 1. If an image I is a binary array, extracting the HLAC features is a very simple operation (namely, counting the number of local patterns in I).

3.2 Formulation

We propose 4D HLAC to represent the features of tesseractic (4D cubic) images in 4D space for pattern recognition in 3D motion. Conditions for the different HLAC variants are summarized in Table 1 ($N = 0,1,2$ and the local $3\times\cdots\times 3$ region for combinations of HLAC dimensions (2, 3, or 4) and values (gray or binary)). In most cases, 3D data in one time frame are provided as a depth image, a voxel image, multi-view camera images, or point clouds. To extract a 4D HLAC feature, the data must be transformed into a voxel image or point clouds. After the time series for these voxels (or point clouds) have been obtained, the 4D HLAC for 3D motion is defined by the following equations:

$$\begin{aligned} h = \sum_{i_x=0}^{M_x}\sum_{i_y=0}^{M_y}\sum_{i_z=0}^{M_z}\sum_{i_t=0}^{M_t} & I_{4D}(D_x i_x, D_y i_y, D_z i_z, D_t i_t) \\ & \cdot I_{4D}(D_x i_x + L_x a_1[1], D_y i_y + L_y a_1[2], \\ & \qquad D_z i_z + L_z a_1[3], D_t i_t + L_t a_1[4])\cdot\ldots \\ & \cdot I_{4D}(D_x i_x + L_x a_N[1], D_y i_y + L_y a_N[2], \\ & \qquad D_z i_z + L_z a_N[3], D_t i_t + L_t a_N[4]) \end{aligned} \tag{3}$$

$$I_{4D}(x,y,z,t) = \begin{cases} 1 & \text{if a tesseract with vertices} \\ & (x,y,z,t),(x+L_x,y,z,t), \\ & \quad \ldots,(x+L_x,y+L_y,z+L_z,t+L_t) \\ & \text{includes at least one point.} \\ 0 & \text{otherwise.} \end{cases} \tag{4}$$

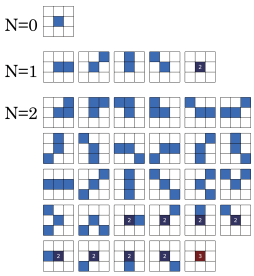

Figure 1: All masks of HLAC for a gray-scale 2D image.

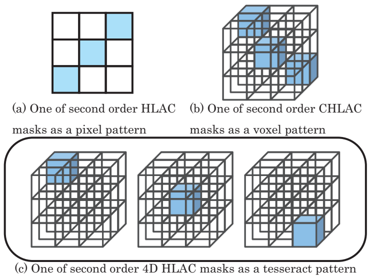

Figure 2: Comparison of HLAC variations.

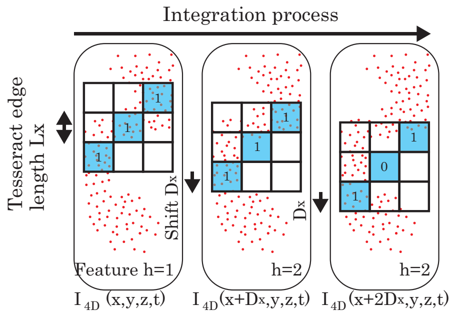

Figure 3: Operation of HLAC from point clouds.

The extraction of 4D HLAC features is executed according to the diagram in Figure 3. The 4D HLAC parameters are as follows:

$L_{x,y,z}$: Tesseract edge length [mm] in space.

L_t : Tesseract edge length [ms] in time.

$D_{x,y,z}$: Shift distance [mm] required to move HLAC mask patterns in space.

D_t : Shift distance [ms] required to move HLAC mask patterns in time.

$A_{x,y,z}$: Analyzed area length [mm] in space.

A_t : Analyzed area duration [ms] in time.

$M_{x,y,z}$: Number of HLAC summations in space ($M_{x,y,z} = \lfloor A_{x,y,z}/D_{x,y,z} \rfloor$).

M_t : Number of HLAC summations in time ($M_t = \lfloor A_t/D_t \rfloor$).

In this study, the sampling rates D_t and L_t were fixed to 33 [ms]. $L_{x,y,z}$ represents the resolution of the pattern. A 4D HLAC feature with small $L_{x,y,z}$ describes the local form and motion in detail, such as the fluctuation of clothes or vibratory movements of a single body part. A 4D HLAC feature with large $L_{x,y,z}$ describes a holistic form and motion of an object, such as the coordination of multiple body parts. When the 3D data is first provided as a voxel time series, the point clouds in the theory are equivalent to voxels.

Voxel time series that are transformed from raw data (e.g., point clouds) may be subjected to temporal subtraction or surface extraction if necessary. Temporal subtraction is intended to emphasize motion by deleting motionless objects, and surface extraction ensures that objects filled by voxels are accounted for, because most of the raw data from 3D depth sensors are regarded as surface patterns. We generally need to test whether such preprocessing is effective for the given purpose.

In this research, rather than gray-scale patterns, we use binary tesseract patterns of spatiotemporal arrays (these can be constructed from point clouds by counting the points in one tesseract). We use binary patterns because the sharp boundaries between objects and void space are transformed into discriminating features. This characteristic is useful in many applications, including human motion recognition. We suggest that gray-scale 4D HLAC should be used for certain types of fluid analysis because of its continuous density gradients.

3.3 Characteristics

Analogous to the original HLAC features, 4D HLAC has the following characteristics:

(a) Model-free. The method does not require any object or world model.

(b) Simple Algorithm. The operations of the method only involve counting local patterns.

(c) Noise Robustness. There is no differential operation such as edge extraction. The integration in the operation of HLAC is expected to eliminate noise analogously to a low-pass filter.

(d) Low Computational Cost and Easy Parallelization. Counting the patterns is a low-cost operation. The algorithm is easily parallelized by arranging the computation of each pattern or separated target area into one process. The parallelization algorithms are discussed in Section 3.4 The computation time of one recognition and the efficiency of the parallelization are discussed in Section 5.

(e) Spatiotemporal Shift Invariant. The integration eliminates the location of the patterns. This invariance makes the recognition robust.

(f) Additivity. The feature vector, including multiple objects and their motion, is the sum of all single feature vectors of the objects and the motions in the image. In Section 4.2, we exploit this characteristic to count action classes with constant computational load.

Table 1: Number of masks for the HLAC variations.

Name	Dimen-sion	Mask size	Mask variation	
			Gray	Binary
HLAC	2D	3×3	35	25
CHLAC	3D	$3 \times 3 \times 3$	279	251
4D HLAC	4D	$3 \times 3 \times 3 \times 3$	2563	2481

(g) High Performance for Pattern Recognition. We show that the performance of our method is very high compared to 2D movie methods (Section 4.1) and to previous 3D methods (Section 5).

3.4 Implementation

Characteristic (d) ensures that 4D HLAC can be effectively parallelized. In this research, we implement 4D HLAC on a single core with a sequential program, a multiple core CPU with OpenMP, and a GPGPU using CUDA. To parallelize the method, we divide the computation into that for a single HLAC pattern and the integrations regarding the time axis. For the HLAC patterns, we developed 2481 CUDA threads to compute the local patterns of binary 4D HLAC on a GPGPU. To avoid redundant computations, we divide the target 4D space along the time axis. When raw data are provided for a moment t, a partial feature vector at $t-1$ is acquired from the data in three time frames $(t, t-1, t-2)$, and this partial feature vector is added to a queue. Finally, the queued partial feature vectors from the time window between $t-1$ and $t-1-M_t$ are summed, and the oldest partial feature vector is deleted from the queue. This algorithm reduces the computation by a factor of $1/M_t$, although the operation is completely equivalent to a one-shot computation for a target time window.

4 BASIC EXPERIMENT

4.1 Classification

4.1.1 Experimental Setup

a In this section, we examine how the 4D HLAC features contribute to the recognition of very simple human arm motions, and compare this to conventional 2D motion analyses. The motion classes for the examination are very simple arm rotations, as shown in Figure 4. These are characterized by movement in the depth and vertical (up-down) directions, so the recognition should exploit information about the location and velocity of the arm movements in 3D space.

Table 2: Test data in the basic classification experiment.

Actors	10
Class of actions	3
Trials of one action by one subject	10
Frame rate	30 [fps]
Frame size for one trial	250 frames (8.3 [s])
Analyzed duration of time frame M_t	20 (666[ms])
Analyzed area $A_{x,y,z}$	$900 \times 900 \times 900$ [mm]
Resolution in 2D images	640×480[pixel]

The data were acquired as RGB-D images from a depth sensor (Microsoft Kinect). The examples of the data acquired from Kinect is shown in Figure 5. The images were transformed into 3D voxel time series, 2D intensity image time series, and 2D depth image time series. Note that 3D voxel data and depth images are theoretically reversible by interconversion. We expect that a comparison between them will indicate how the real-world structure in the spatiotemporal domain contributes to motion recognition, even when the structure is only captured from one perspective.

We set $L_{x,y,z}$= 10, 20, 30, and 50 [mm], L_t=33 [ms], and $D_{x,y,z,t} = L_{x,y,z,t}$ in all analyses. The time frame was $M_t = 20$ frames. In the classification part, we used Fisher's Discriminant Analysis (FDA) for dimension reduction and the Minimum Distance Classifier. Features were extracted at each point by sliding the time window, and the classifier assigned one of the action classes to the current feature.

We applied the CHLAC feature to depth movies and intensity movies (Figure 6). The backgrounds were eliminated from these movies based on depth information. For the CHLAC feature in this examination, the auto-correlation order was $N = 0, 1, 2$, and the range of displacements a_i was within a $3 \times 3 \times 3$ local region. The 2D image resolution was scaled to 1, 0.5, 0.3, 0.2, and 0.1 times that of the original image. This change of resolution is equivalent to changing the voxel size. Edge extraction was based on the Canny Method (Canny, 1986), with parameter values of 50, 250, or 450. All parameter combinations were applied to determine the combination that produced the best result.

We collected the test data for the examination under the conditions listed in Table 2. The classification rate was calculated by leave-one-actor-out (LOAO) cross-validation, whereby the correct recognition rates for one actor's actions are calculated after the recognition system is learned from the other actors' actions. Finally, we calculated the average and

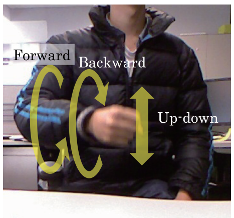

Figure 4: Motion classes in the basic experiments.

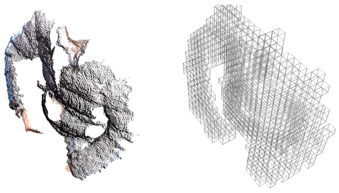

(a) (b)

Figure 5: Data types of 3D movies: (a) Point cloud data (b) Binary voxel data.

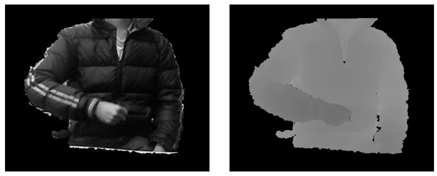

(a) (b)

Figure 6: Images used in the comparative experiment: (a) Intensity image (b) Depth image.

standard deviation of the recognition rates for all actors.

4.1.2 Results

The experimental results are shown in Figure 7. From the 4D HLAC experiments, the best classification rate was 98.2% for the smallest voxel size (10 [mm]). Temporal subtraction before 4D HLAC produced almost the same performance as without subtraction. This implies that 4D HLAC can extract features appropriate to movement.

Using CHLAC, 2D intensity and depth movies induce worse performance than 3D movies with 4D HLAC, even when both movies have exactly the same perspective. The best classification rates were 63.5% for intensity movies and 75.8% for depth movies. The results from intensity movies are better than the chance level (33%), but worse than the results from depth movies and voxel movies. This indicates that the real-world structure in 3D space is critical for the recognition, even when only one perspective is used and the image includes some occlusion.

Although depth movies are supposed to contain the same information as voxel movies, feature extraction from depth movies using CHLAC is worse than that from voxel movies by 4D HLAC. The reasons for this low performance with depth movies are as follows:

Boundary Effect. The boundaries between a moving arm and a body trunk are taken into account, whereas physically distant body parts do not contribute.

Depth Direction. The motion along the depth axis in depth movies is represented by the change of gradient in the depth value. However, temporal changes in gradient are difficult to capture.

We believe the reasons above can be applied to any other 2D image descriptors for depth movies.

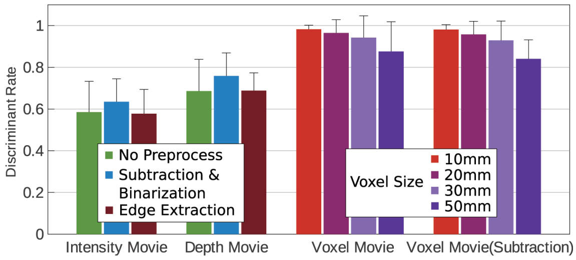

Figure 7: Results of the discrimination experiment.

Figure 8: Simultaneous actions by three actors.

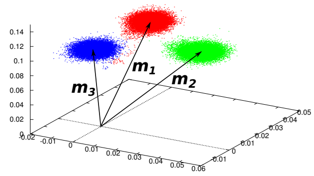

Figure 9: The discriminant space with zero-motion for decomposition of the three motions.

4.2 Counting

4.2.1 Theory and Experimental Setup

To demonstrate the usefulness of the additivity property, we constructed an algorithm to count target motions with a computational cost that is independent of the number of actions in the target area.

The HLAC vectors h are interpreted as:

$$h \approx n_1 m_1 + n_2 m_2 + \ldots + n_C m_C + \varepsilon, \qquad (5)$$

where $m_1, m_2, \ldots, m_C$ are the average feature vectors of the respective action classes, $n_1, n_2, \ldots, n_c$ are the number of actions, and ε is a vector of common elements in all classes. The lengths of the decomposed vectors $n_1, n_2, \ldots, n_C$ based on the base vectors $m_1, m_2, \ldots, m_C$ represent the number of actions if the acquired h can be decomposed into vectors $n_1 m_1, n_2 m_2, \ldots, n_C m_C$.

To estimate the number of classes, we must calculate the inverse of Equation (5) from h to $n = (n_1, n_2, \ldots, n_C)$. To estimate the inverse function, we propose the following algorithm.

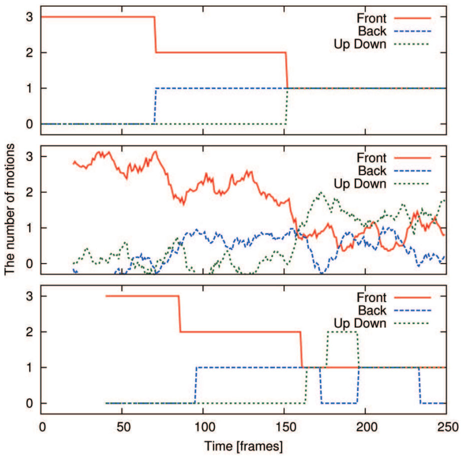

Figure 10: Results of the counting experiment. Top: Ground truth; Middle: Estimated motion numbers; Bottom: Discretized estimated motion numbers.

1. Suppress the feature space with all target action data and common action ε using FDA. The dimension of the suppressed feature vector is the number of classes C.
2. Transform the average vectors of action classes $m_1, m_2, \ldots, m_C$ into the FDA space $\hat{m}_1, \hat{m}_2, \ldots, \hat{m}_C$.
3. Calculate the inverse matrix of $(\hat{m}_1 - \hat{\varepsilon}\ \hat{m}_2 - \hat{\varepsilon}\ \ldots\ \hat{m}_C - \hat{\varepsilon})$.
4. Estimate the vector of the number of actions.
$$\begin{aligned} &\left(n_1\ n_2\ \cdots\ n_C\right)^T \\ &= (\hat{m}_1 - \hat{\varepsilon} \quad \hat{m}_2 - \hat{\varepsilon} \quad \ldots \quad \hat{m}_C - \hat{\varepsilon})^{-1}\hat{h}, \end{aligned} \tag{6}$$
where $\hat{h}$ is transformed from the feature vector h into FDA space.
5. Discretize $(n_1 n_2 \ldots n_C)^T$ using a rounding function.

We adopt the zero-vector as the common vector ε after applying temporal subtraction to the voxel time series; temporal subtraction for an unchanged time series results in 0. The inverse function can be estimated using multiple regression and a pseudoinverse. However, these methods require training data with all possible combinations of actions in the learning phase, whereas the proposed method only requires training data from one action with one label.

We used the data from the previous experiment to learn the average class vectors m_i, and conducted an experiment with three actors to estimate the number of action classes (Figure 8). $L_{x,y,z}$ and $D_{x,y,z}$ were set to 30 [mm].

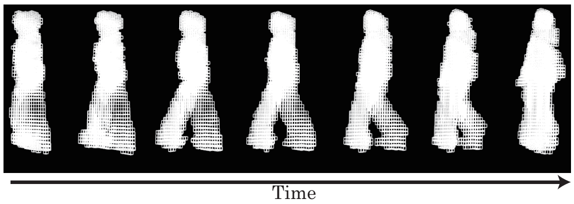

Figure 11: Example of a walking pattern in the voxel time series of the IXMAS dataset.

4.2.2 Results

The training data in the compressed feature space for the three motions are shown in Figure 9. The motion counting results are shown in Figure 10. We calculated the simple moving averages, and rounded these to give $(n_1 n_2 \ldots n_C)^T$. The results show that the estimated number of motions follows the actual number.

An additional experiment showed that a smaller voxel size (10 [mm]) produces a worse result. Generally, smaller voxel sizes are too sensitive to small irrelevant motion or measurement noise. For instance, in this experiment, the third person was further away from the measuring instrument than in the discriminant experiment; thus, bigger voxels (30 [mm]) gave better results.

5 IXMAS DATASET

5.1 Experimental Setup and Method

To compare 4D HLAC to previous 3D motion recognition techniques, we applied the proposed method to the IXMAS dataset (Weinland et al., 2006). This dataset has been used for various studies into pattern recognition in 3D motion. We shall demonstrate the advantages of our method in terms of recognition performance and computational cost.

The IXMAS dataset consists of multi-view camera movies and voxel time series. The voxel time series data are applicable to our method (Figure 11). The multi-view camera system ensures there is no critical occlusion in the data, unlike in the previous section. The inside of each object is filled by voxels, with the length of each voxel edge estimated to be 30–40 [mm] (this edge length is not explicitly specified, but is not important for this experiment).

To recognize motion in any direction, we generate additional training data by rotating the original training data around the vertical axis in 15° steps. Rotation invariance can be ensured by making a new feature vector as the sum of all the rotated feature vectors.

Table 3: Computational time of 4D HLAC for IXMAS dataset; M_t=20 [frames].

Implementation [a]	Time [ms]	
	One shot[b]	Queue and sum[c]
CPU (Single thread)	6346	317
CPU (12 threads)	932	46
GPGPU (2481 CUDA threads)	183	9

[a] CPU: Intel Core i7-3930K 3.2 Hz (6 cores), GPU: GeForce GTX 680 (1536 cores), Memory: 31.4GB, OS: Ubuntu 12.04 64bit. [b] "One shot" represents consumed time for the calculation of a HLAC feature vector for 20 frames at one time. [c] "Queue and sum" represents the computation time using the algorithm with a queue of partial feature vectors.

Contrary to our expectation, the results from this operation are almost the same, or slightly worse, than the strategy with additional rotated training data for learning and original features for recognition.

When examining the performance of 4D HLAC, we must evaluate the following conditions for the extraction of features:

Effect of Surface. In most cases, a 3D range sensor provides information about the object surface. We utilize the voxel data format with and without surface extraction.

Independent Analysis of Upper and Lower Bodies. Generally, HLAC eliminates any locations in which a HLAC pattern occurs, whereas human whole-body motion consists of independent or dependent multi-body motion. Independent motion should be analyzed independently for precise recognition. We split the analyzed area into the upper and lower body, divided at the central horizontal plane. The height of this plane is defined by the average mid-points of the distance between the highest and lowest voxels for the analyzed time frame M_t. Under this splitting condition, the feature vector has 4962 elements (2481×2).

Detail of Motion. We varied $L_{x,y,z}$ to adjust the granularity of the motion details in order to correctly capture the coordination among body parts.

We utilize a linear support vector machine (LSVM) to classify the actions after FDA is applied to the 4D HLAC feature vectors. The recognition in each trial is determined by a majority vote of the system recognition in every frame while the system recognizes the behavior in a frame based on the last 20 frames (M_t).

5.2 Results

Under the above experimental conditions, we obtained the results listed in Table 5. Our method achieved an optimal recognition rate of 95.5%.

When using the additional data generated by rotating the original data, the distribution of training samples from a certain action class forms a closed curve in the feature space. Regardless of such a non-normal distribution, the experimental results are good, even those from the linear classification method, because the feature vectors of actions in the feature space are significantly separated. This indicates that our method can capture the effective features of actions from the raw voxel time series.

Table 4 gives the confusion matrix. The most confusing actions are the hand-waving and head-scratching actions. Both actions consist of hand shaking movements. The reason for the misrecognition is that contact between a hand and the head is very difficult to detect, because the local patterns at the contact points can easily be occluded.

Table 3 gives the computational time needed to compute the feature for the most effective condition. The fastest time of 9 [ms] for one time classification was given by GPGPU parallelization, while CPU parallelization is also effective (46 [ms]). The classification method combining FDA and LSVM takes only a few microseconds because it consists of only linear calculations.

To compare our method with previous methods, the LOAO performance of some state-of-the-art methods is given in Table 6. Although the recognition rate is a good performance indicator, it is not easy to compare the recognition rates of each method because of their different experimental conditions. According to Table 6 and Table 3, our method outperforms those previous methods that reported a computation time, demonstrating that the computational cost of our method is very competitive.

Among all methods, the performance of our method is third behind those of Holte et al. (2012) and Turaga et al. (2008). Neither of these studies reported a computational cost, though Turaga et al. argued that their method was computationally efficient. The method of Holte et al. may have a much higher computational cost than our method, as it relies on a complicated algorithm to produce the highest recognition rate (100%). Turaga et al. proposed a classification method based on statistical manifold learning with a 3D motion feature (Weinland et al., 2006), and reported a slightly higher performance rate than our method. This indicates that our method can be improved by a further appropriate classification technique.

Table 4: Confusion matrix for IXMAS dataset: mask size $L_{x,y,z} = 4$; average recognition rate = 95.5%; $(\cdot)$ represents the number of trials recognized as each action class in 36 samples (12 actors $\times$ 3 trials).

Recognized actions	Performed actions										
	Check watch	Cross arm	Scratch head	Sit down	Get up	Turn around	Walk	Wave hand	Punch	Kick	Pick up
Check watch	**94.4(34)**	0.0(0)	0.0(0)	0.0(0)	0.0(0)	0.0(0)	0.0(0)	0.0(0)	0.0(0)	0.0(0)	0.0(0)
Cross arm	5.6(2)	**100.0(36)**	2.8(1)	0.0(0)	0.0(0)	0.0(0)	0.0(0)	2.8(1)	0.0(0)	0.0(0)	0.0(0)
Scratch head	0.0(0)	0.0(0)	**97.2(35)**	0.0(0)	0.0(0)	0.0(0)	0.0(0)	16.7(6)	0.0(0)	0.0(0)	0.0(0)
Sit down	0.0(0)	0.0(0)	0.0(0)	**100.0(36)**	0.0(0)	0.0(0)	0.0(0)	0.0(0)	0.0(0)	0.0(0)	2.8(1)
Get up	0.0(0)	0.0(0)	0.0(0)	0.0(0)	**100.0(36)**	0.0(0)	0.0(0)	0.0(0)	0.0(0)	0.0(0)	0.0(0)
Turn around	0.0(0)	0.0(0)	0.0(0)	0.0(0)	0.0(0)	**100.0(36)**	5.6(2)	0.0(0)	0.0(0)	0.0(0)	0.0(0)
Walk	0.0(0)	0.0(0)	0.0(0)	0.0(0)	0.0(0)	0.0(0)	**88.9(32)**	0.0(0)	0.0(0)	0.0(0)	0.0(0)
Wave	0.0(0)	0.0(0)	0.0(0)	0.0(0)	0.0(0)	0.0(0)	0.0(0)	**80.6(29)**	5.6(2)	0.0(0)	0.0(0)
Punch	0.0(0)	0.0(0)	0.0(0)	0.0(0)	0.0(0)	0.0(0)	0.0(0)	0.0(0)	**91.7(33)**	0.0(0)	0.0(0)
Kick	0.0(0)	0.0(0)	0.0(0)	0.0(0)	0.0(0)	0.0(0)	2.8(1)	0.0(0)	2.8(1)	**100.0(36)**	0.0(0)
Pick up	0.0(0)	0.0(0)	0.0(0)	0.0(0)	0.0(0)	0.0(0)	2.8(1)	0.0(0)	0.0(0)	0.0(0)	**97.2(35)**

Table 5: LOAO recognition rate [%] for IXMAS dataset with different feature extraction conditions; $L_{x,y,z}$ is voxel size in the IXMAS format.

$L_{x,y,z}$	Whole body		Separated into upper and lower bodies	
	Filled	Surface	Filled	Surface
1	84.3 %	81.1 %	87.4 %	89.1 %
2	91.2 %	88.1 %	94.4 %	90.7 %
3	90.9 %	91.9 %	94.7 %	92.7 %
4	92.7 %	91.7 %	93.7 %	95.5 %
5	93.4 %	91.4 %	91.9 %	93.2 %
6	92.2 %	92.7 %	90.7 %	90.7 %

Table 6: Comparison with 3D human action recognition approaches. The results for the LOAO cross-validation were obtained using the IXMAS dataset. 'Dim.' denotes data dimension used in the IXMAS dataset.

Approach	Actions	Actors	Dim.	Rate [%]	time [ms]
(Wu et al., 2011)	12	12	2D	89.4	N/A
(Pehlivan and Duygulu, 2010)	11	10	3D	90.9	N/A
(Weinland et al., 2006)	11	10	3D	93.3	N/A
(Cilla et al., 2013)	11	10	2D	94.0	N/A
(Turaga et al., 2008)	11	10	3D	98.8	N/A
(Holte et al., 2012)	13	12	3D	100	N/A
(Cherla et al., 2008)	13	N/A	2D	80.1	50
(Weinland et al., 2010)	11	10	2D	83.5	2∼
(Chaaraoui et al., 2014)	11	12	2D	91.4	5
4D HLAC approach	11	12	3D	95.5	*

* Computational costs of some implementation are shown in Table 3

6 CONCLUSION

In this article, we have proposed 4D HLAC for 3D motion recognition. Our experimental results reinforce the simplicity and low computational cost of the proposed method, as well as its general versatility and performance. We conclude that 4D HLAC is a highly capable and computationally efficient 3D motion recognition technique.

The next steps for the research are to extend multi resolution analysis of 4D pattern from the split analysis in IXMAS experiment, to improve the classification algorithm appropriate for 4D HLAC and apply it to practical applications.

ACKNOWLEDGEMENTS

The work reported in this paper has been supported by Grant-in-Aid Nos. 24680024, 24119001, and 24000012 from the Ministry of Education, Culture, Sports, Science and Technology, Japan.

REFERENCES

Canny, J. (1986). A computational approach to edge detection. *IEEE Transactions on pattern analysis and achine intelligence*, pages 679–714.

Chaaraoui, A. A., Padilla-Lopez, J. R., Ferrandez-Postor, F. J., Nieto-Hidalgo, M., and Florenz-Revuelta, F. (2014). A vision-based system for intelligent monitoring: human behaviour analysis and privacy by context. *Sensors*, 14:8895–8925.

Cherla, S., Kulkarni, K., Kale, A., and Ramasubramanian, V. (2008). Towards fast, view-invariant human action recognition. In *Proc. of the IEEE Conf. on Computer Vision and Pattern Recognition Workshops*.

Cilla, R., Patricio, M. A., Berlanga, A., and Molina, J. M. (2013). Human action recognition with sparse classification and multiple-view learning. *Expert Systems*.

Holte, M., Chakraborty, B., Gonzalez, J., and Moeslund, T. (2012). A local 3-d motion descriptor for multi-view human action recognition from 4-d spatio-temporal interest points. *IEEE Journal of Sellected Topics in Signal Process*, 6:553–565.

Kanezaki, A., Harada, T., and Kuniyoshi, Y. (2010). Partial matching of real textured 3d objects using color cubic higher-order local auto-correlation features. *The Visual Computer*, 26(10):1269–1281.

Kobayashi, T. and Otsu, N. (2004). Action and simultaneous multiple-person identification using cubic higher-order local auto-correlation. In *Proc. of 17th ICPR*, pages 741–744.

Otsu, N. and Kurita, T. (1988). A new scheme for practical flexible and intelligent vision systems. *Proceedings of IAPR Workshop on Computer Vision*, pages 431–435.

Pehlivan, S. and Duygulu, P. (2010). A new pose-based representation for recognizing actions from multiple cameras. *Computer Vision and Image Understanding*, 115:140–151.

Turaga, P., Veeraraghavan, A., and Chellappa, R. (2008). Statistical analysis on stiefel and grassmann manifolds with applications in computer vision. In *Proc. of the IEEE Conf. on CVPR*.

Weinland, D., Ozuysal, M., and Fua, P. (2010). Making action recognition robust to occlusions and viewpoint changes. In *Proc. of ECCV*.

Weinland, D., Ronfard, R., and Boyer, E. (2006). Free viewpoint action recognition using motion history volumes. *Computer Vision and Image Understanding*, 104(2–3):249–257.

Wu, X., Xu, D., Duan, L., and Luo, J. (2011). Action recognition using context and appearance distribution features. In *Proc. of the IEEE Conf. on CVPR*, pages 489–496.